THE JOURNAL OF BIOLOGICAL CHEMISTRY VOL. 291, NO. 13, pp. 7142–7155, March 25, 2016
Published in the U.S.A.

Arf-like Protein 3 (ARL3) Regulates Protein Trafficking and Ciliogenesis in Mouse Photoreceptors*

Received for publication, December 16, 2015, and in revised form, January 22, 2016 Published, JBC Papers in Press, January 25, 2016, DOI 10.1074/jbc.M115.710954

Christin Hanke-Gogokhia[‡§], Zhijian Wu[¶], Cecilia D. Gerstner[‡], Jeanne M. Frederick[‡], Houbin Zhang[‖1], and Wolfgang Baehr[‡ ‡‡§§2]**

From the [‡]Department of Ophthalmology and Visual Sciences, John A. Moran Eye Center, and [‡‡]Department of Neurobiology and Anatomy, University of Utah School of Medicine, Salt Lake City, Utah 84132, the [§]Department of Biochemistry and Biology, University of Potsdam, 14476 Potsdam-Golm, Germany, the [¶]NEI, National Institutes of Health, Bethesda, Maryland 20892, the [‖]Sichuan Provincial Key Laboratory for Human Disease Gene Study, Institute of Laboratory Medicine, Hospital of University of Electronic Science and Technology of China and Sichuan Provincial People's Hospital, Chengdu, 610072 Sichuan, China, the [**]School of Medicine, University of Electronic Science and Technology of China, Chengdu, 610072 Sichuan, China, and the [§§]Department of Biology, University of Utah, Salt Lake City, Utah 84112

Arf-like protein 3 (ARL3) is a ubiquitous small GTPase expressed in ciliated cells of plants and animals. Germline deletion of *Arl3* in mice causes multiorgan ciliopathy reminiscent of Bardet-Biedl or Joubert syndromes. As photoreceptors are elegantly compartmentalized and have cilia, we probed the function of ARL3 (ADP-ribosylation factor (Arf)-like 3 protein) by generating rod photoreceptor-specific (prefix ^{rod}) and retina-specific (prefix ^{ret}) *Arl3* deletions. In predegenerate $^{rod}Arl3^{-/-}$ mice, lipidated phototransduction proteins showed trafficking deficiencies, consistent with the role of ARL3 as a cargo displacement factor for lipid-binding proteins. By contrast, $^{ret}Arl3^{-/-}$ rods and cones expressing Cre recombinase during embryonic development formed neither connecting cilia nor outer segments and degenerated rapidly. Absence of cilia infers participation of ARL3 in ciliogenesis and axoneme formation. Ciliogenesis was rescued, and degeneration was reversed in part by subretinal injection of adeno-associated virus particles expressing ARL3-EGFP. The conditional knock-out phenotypes permitted identification of two ARL3 functions, both in the GTP-bound form as follows: one as a regulator of intraflagellar transport participating in photoreceptor ciliogenesis and the other as a cargo displacement factor transporting lipidated protein to the outer segment. Surprisingly, a farnesylated inositol polyphosphate phosphatase only trafficked from the endoplasmic reticulum to the Golgi, thereby excluding it from a role in photoreceptor cilia physiology.

Photoreceptor outer segments (OS)[3] are modified primary cilia specializing in phototransduction (1). Polypeptides involved in phototransduction (2) are transmembrane proteins (*e.g.* rhodopsin) or peripheral membrane (PM) proteins (*e.g.* transducin and PDE6 (cGMP phosphodiesterase 6)). We are interested how PM proteins traffic from the inner segment (site of biosynthesis) through a narrow connecting cilium to the outer segment (site of phototransduction). PM proteins participating in signaling are rhodopsin kinase (GRK1, G protein receptor kinase 1) (3, 4), the heterotrimeric G protein transducin ($T\alpha\beta\gamma$) (5–8), and heterotetrameric cGMP phosphodiesterase ($PDE6\alpha\beta\gamma\gamma$) (9, 10). These proteins are soluble but lipidated (prenylated or acylated) for membrane attachment (11–16). Attachment of lipidated proteins peripherally facilitates two-dimensional diffusion for rapid interactions during phototransduction (17, 18).

Replacement of entire outer segments every 10 days in mice necessitates efficient trafficking of membrane-associated proteins (19, 20). Lipidated proteins associate transiently with the endoplasmic reticulum (ER) where post-translational processing occurs (21). Trafficking to the outer segment by diffusion requires solubilization factors that interact with lipid side chains, *e.g.* PDEδ (also known as PrBP/δ or PDE6D, a prenyl-binding protein originally thought to be a subunit of PDE6) (22, 23) and UNC119 paralogs (UNC119a and UNC119b, where UNC119 is uncoordinated 119, a human *Caenorhabditis elegans* homolog) (24). PDEδ is a prenyl-binding protein that interacts with C-terminal farnesyl and geranylgeranyl lipids, whereas UNC119 is an acyl-binding protein specific for N-terminal C-12 and C-14 fatty acids. *PDE6D* null mutations in human are associated with Joubert syndrome (25), caused by impaired ciliary targeting of INPP5E (inositol polyphosphate-5-phosphatase E), an enzyme thought to mediate ciliary stabi-

* This work was supported in part by National Institutes of Health Grants EY08123 and EY019298 (to W. B.) and NEI Core Grant EY014800-039003, unrestricted grants to the University of Utah Department of Ophthalmology from Research to Prevent Blindness (New York), National Science Foundation of China Grant 81371030, and Science and Technology Department of Sichuan Grant 2014HH0009 (to H. Z.). The authors declare that they have no conflicts of interest with the contents of this article. The content is solely the responsibility of the authors and does not necessarily represent the official views of the National Institutes of Health.

[1] To whom correspondence may be addressed. E-mail: houbin.zhang@gmail.com.

[2] Recipient of a Research to Prevent Blindness Senior Investigator Award, a Research to Prevent Blindness Nelson Trust Award, and an award from the Retina Research Foundation (Alice McPherson, MD), Houston, TX. To whom correspondence may be addressed: Moran Eye Center, University of Utah, 65 Mario Capecchi Dr., Salt Lake City, UT 84132. Tel.: 801-585-6643; E-mail: wbaehr@hsc.utah.edu.

[3] The abbreviations used are: OS, outer segment; AAV, adeno-associated virus; BB, basal body; CC, connecting cilium; CDF, cargo displacement factor; Cre, Cre recombinase; ER, endoplasmic reticulum; ERG, electroretinogram; GAP, GTPase-activating protein; GEF, guanosine nucleotide exchange factor; IFT, intraflagellar transport; IS, inner segment; OCT, optical coherence tomography; OKT, optokinetic tracking; ONL, outer nuclear layer; PM, peripheral membrane; EGFP, enhanced GFP; T, transducin; P, postnatal day; h, human; RP, retinitis pigmentosa; PI4P, phosphatidylinositol 4-phosphate; cd, candela.

lization (26). Deletion of *Pde6d* in mice produced retinal degeneration caused by trafficking defects of GRK1 and PDE6 (22). A missense mutation in *UNC119* is associated with cone-rod dystrophy (27).

ARL3 (ADP-ribosylation factor (Arf)-like 3 protein) is a soluble, small GTPase that has been identified in all ciliated organisms (28). Mammalian ARL3 was identified as an expressed sequence tag (EST) and shown to be present in a number of human tissues and tumor cell lines (29). Cilia function was identified first in the protozoon *Leishmania donovani* (30). Experiments in ciliated hTert-RPE and IMCD3 cells (31), pulldowns (32–34), and crystallography (35–38) identified Arf-like (ARL) proteins ARL2 and ARL3 as interactants of PDEδ and UNC119 (31, 38, 39). ARL3 localizes to the photoreceptor synaptic terminal, cell body, inner segment, and connecting cilium (40) and colocalizes with RP2 (retinitis pigmentosa protein 2) (41), UNC119 (42), and PDEδ (22). ARL3 GTPase activity is regulated by a guanosine nucleotide exchange factor (GEF) and a GTPase-activating protein (GAP). RP2 functions as an ARL3 GAP, and ARL13b was identified recently as an ARL3 GEF enabling GTP/GDP exchange at ARL3-GDP (43). Mutations in ARL13b in human and mouse are associated with Joubert syndrome (44, 45). *In vitro* experiments identified ARL3-GTP as a guanosine nucleotide dissociation inhibitor displacement factor, and for simplicity it is referred to as cargo displacement factor (CDF). A germline *Arl3* knock-out in mice revealed syndromic ciliopathy in that $Arl3^{-/-}$ mice did not survive beyond postnatal week 3 and sustained ciliopathy in kidney, liver, and pancreas in addition to photoreceptor degeneration (46).

We generated rod-specific and retina-specific *Arl3* knockouts to study defects in photoreceptor protein trafficking. In $^{rod}Arl3$ knock-outs, Cre recombinase, an enzyme carrying out site-specific recombination, is expressed post-ciliogenesis allowing formation of outer segments, whereas in $^{ret}Arl3$ knock-outs, Cre is expressed during embryonic development. The results show that ER to OS trafficking of lipidated OS proteins in $^{rod}Arl3^{-/-}$ retina was impaired, leading to outer segment shortening and slow retinal degeneration, consistent with loss of CDF function. The $^{ret}Arl3^{-/-}$ photoreceptors formed neither connecting cilia nor outer segment membrane, leading to protein accumulation in the inner segment and rapid degeneration. INPP5E, which localizes exclusively to the Golgi apparatus of WT photoreceptors, was significantly reduced in $^{ret}Arl3^{-/-}$ inner segments suggesting that trafficking of INPP5E from ER-to-Golgi is ARL3-dependent.

Experimental Procedures

Animals—All procedures were approved by the University of Utah Institutional Animal Care and Use Committee and were conducted in compliance with the Guide for Care and Use of Laboratory Animals from National Institutes of Health. Mice were maintained in a 12:12-h dark/light cycle. *Flp* mice were used to invert the gene trap at FRT sites. Six3-Cre and iCre75 transgenic mice were used to generate retina- and rod-specific *Arl3* knock-outs (Fig. 1) (47–49). A transgenic mouse expressing the EGFP-CETN2 fusion protein (JAX stock no. 008234) was used to identify centrioles with fluorescence microscopy (50).

Generation of Arl3 Gene Knock-out Mouse—A mouse embryonic stem cell line containing a gene trap cassette in intron 1 of the *Arl3* gene was purchased from the European Mouse Mutant Cell Repository (EUCOMM, Helmholtz Zentrum München, Germany). The gene trap was flanked by antisense FRT and loxP sites facilitating trap inversion (51, 52) by *Flp*- and Cre-induced recombination (Fig. 1, *B–D*). The presence of the gene trap and the integrity of short and long arms were verified by PCR. Chimeric mice were generated by the transgenic mouse core facility, University of Utah. The WT allele was genotyped by PCR using primer pair ARL3-F1 (5′-AGACCACGTGCTCTTCCATC) and ARL3-R3 (5′-GTGGTTATGTGTTGTCATGAG), yielding a 367-bp amplicon. The presence of the gene trap was verified using primer pair ARL3-F1 and RP2-R5 (5′-CTAGACAATCGGACAGACAC), yielding a 1080-bp amplicon. Heterozygous *Arl3* germline knock-out mice ($Arl3^{GT/+}$) were outbred to *Flp* mice to invert the gene trap at FRT sites. *Flp*-FRT recombination (53) was verified using the primer pair RP2-R5 and Eu-R2 (5′-CTTGAACCTCCTCGTTCGAC), yielding an ~500-bp amplicon. Mice carrying the inverted gene trap (floxed mice) were mated with transgenic mice expressing Cre to generate conditional knock-outs. Cre-loxP recombination was checked with a Cre-specific primer set. The iCre75 transgene was identified using the primer pair iCre75-F (5′-GGATGCCACCTCTGATGAAG) and iCre75-R (5′-CACACCATTCTTTCTGACCCG). Six3-Cre mice were genotyped using the primer pair Six3Cre159 (5′-TCGATGCAACGAGTGATGAG) and Six3Cre160 (5′-TTCGGCTATACGTAACAGGG). Absence of the *rd8* mutation was confirmed by PCR (54).

ARL3 Antibody Generation—Full-length recombinant ARL3 was prepared as described (41). Rabbit anti-ARL3 polyclonal antibody was prepared by Covance (LabCorp), Research Triangle Park, NC, using recombinant ARL3 as immunogen. ARL3 antibody was purified from bleeds using affinity chromatography on GST-ARL3. GST-ARL3 was prepared as described (41).

Confocal Immunohistochemistry—All animals were dark-adapted overnight. Retina cryosections were prepared as described (55). Sections were incubated with the following polyclonal primary antibodies: VPP (anti-rhodopsin, 1:500) (56); anti-rod Tα (anti-transducin-α, 1:500, Santa Cruz Biotechnology); anti-M/L-opsin (1:500, Chemicon); anti-S-opsin (1:500, Chemicon); MOE (anti-rod PDE6, 1:500, Cytosignal); Tβγ (anti-transducin-βγ, 1:500, Cytosignal); Rab28 (goat, 1:200, Biorbyt); ARL13b (1:200, ProteinTech); and anti-Giantin (1:100, Abcam). Monoclonal antibodies included the following: G8 (anti-GRK1, 1:500, Santa Cruz Biotechnology); IS4 (anti-guanylate cyclase 1, 1:500, from Dr. Kris Palczewski, Case Western Reserve); and CNGA1/3 (anti-cGMP-gated ion channel, 1:500, NeuroMab). Alexa488- or Alexa555-conjugated goat anti-rabbit, Cy3-conjugated goat anti-mouse, and Cy3-conjugated donkey anti-goat secondary antibodies were diluted 1:1000. Images were acquired using an Olympus Fluoview 1000 confocal microscope.

Immunoblotting—Proteins of retina lysates were separated by SDS-12.5% PAGE and transferred to a nitrocellulose membrane processed as described (55). Primary antibodies were diluted 1:500 for anti-ARL3 and 1:1000 for anti-β-actin (Sigma)

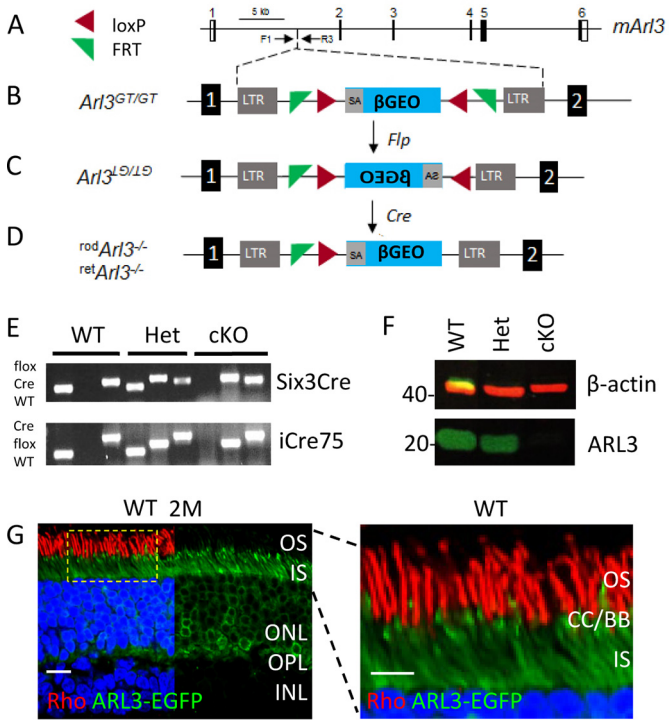

FIGURE 1. **Generation of *Arl3* conditional knock-out mice.** *A,* schematic of the mouse *Arl3* gene (*mArl3*) with its six exons. *B,* gene trap was inserted in intron 1 leading to an early termination of ARL3 translation. $Arl3^{GT/GT}$, homozygous gene-trapped mice. *LTR*, long terminal repeat; *SA*, splice acceptor site. *β-GEO*, composite of the reporter β-galactosidase and the neo cassette, main components of the gene trap. *C,* diagram of the inverted gene trap following recombination with *Flp* at FRT sites. *D,* schematic of the reverted gene trap after Cre-induced recombination, generating rod- or retina-specific knock-outs. *E,* genotyping of WT, heterozygous, and homozygous mice, showing $^{ret}Arl3^{-/-}$ (*top panel*) and $^{rod}Arl3^{-/-}$ (*bottom panel*). For detail, see "Experimental Procedures." *F,* immunoblot. ARL3 protein is absent in the homozygous conditional knock-out (*cKO*) at 2 months; β-actin is a loading control. *G,* distribution of ARL3 in photoreceptors. ARL3-EGFP was expressed by subretinal injection of scAAV2/8 virus. ARL3 protein localizes in the CC/BB area, IS, and ONL of WT photoreceptors. Rhodopsin of rod OS was labeled by VPP-rho antibody (*red*). *Scale bar,* 10 μm. Enlargement of the *dotted area* is shown, *right*. *Scale bar,* 5 μm.

in 1× TTBS containing 5% milk. After incubation overnight at 4 °C, membranes were incubated for 1 h at room temperature with the following secondary antibodies (Odyssey): iR680 goat anti-mouse (1:5000) and iR800 goat anti-rabbit (1:3000). Images were acquired using an Odyssey scanner.

Electroretinography (ERG)—ERGs were measured as described (41) with minor modifications. Single-flash scotopic responses were recorded at stimulus intensities of −40 db (−3.4 log cds·m^{-2}) to 20 db (2.39 log cds·m^{-2}). For photopic ERGs, the mice were light-adapted under background light of 1.48 log cds·m^{-2} for 5–10 min. Single-flash responses were recorded at stimulus intensities of −10 db (−0.6 log cds·m^{-2}) to 20 dB (2.39 log cds·m^{-2}).

OptoMotry (OKT)—Optomotor reflex-based tests were performed using an OptoMotry system (Cerebral Mechanics). Rotation speed (12°/s) and contrast were kept constant as described (57). The mice were adapted to room light (150–250 lux), and OptoMotry was performed under light conditions to test cone-mediated vision.

Optical Coherence Tomography (OCT)—Mice were anesthetized initially by inhalation of 3% isoflurane/O_2 mixture (flow rate of 1.0 liter/min) in a closed canister, and anesthesia was maintained with 1.5% isoflurane/O_2 mixture at the same flow rate. After each mouse was transferred to a heated water pad (37 °C), pupils were dilated with a 1% tropicamide solution, and corneas were hydrated periodically with 1× PBS, pH 7.4, to prevent corneal desiccation. Images were acquired from both eyes using a 30° lens and Heidelberg Retina Angiograph-optical coherence tomography (Spectralis Heidelberg, Germany) with a 488-nm argon blue laser and standard 500-nm long-pass filter. The mice were transferred to a recovery heat pad maintained at 37 °C and monitored until fully conscious.

EGFP-INPP5E Construct and Neonatal Electroporation—The mouse *Inpp5e* gene was amplified from the cDNA prepared from mouse retina using the primer pair of 5′-ATGCCATCCAAGTCAGCTTGC (forward) and 5′-CATCCTTTGCAGTGACCTTGG (reverse). *Inpp5e* cDNA was cloned into a pEGFP-C1 vector (Clontech) that was amplified with the primer pair of 5′-GCCAAGGTCACTGCAAAGGATGCAGCCATACCACATTTGTAGAG (forward) and 5′-CAGGCAAGCTGACTTGGATGGCATCTTGTACAGCTCGTCCATG (reverse). The *Inpp5e* cDNA was ligated to the vector DNA using a NeBuilder kit (New England Biolabs). INPP5E was fused in-frame to the C terminus of EGFP and verified by sequencing. The EGFP-INPP5E-expressing plasmid was introduced into photoreceptors of neonatal mice using *in vivo* electroporation (41), and postnatal day 15 (P15) mouse eyes were harvested for immunohistochemistry.

Generation of ARL3-EGFP Shuttle Vector and AAV (scAAV-ARL3-EGFP)—Recombinant self-complementary AAV2/8 (scAAV2/8) was used to express ARL3-EGFP under the control of the *Grk1* promoter. Mouse *Arl3* was cloned into a scAAV shuttle vector, pscAAV-CAG-EGFP (provided by W. W. Hauswirth), to generate scAAV2/8 packaging construct scAAV-ARL3-EGFP. To make a self-complementary AAV vector, the left ITR (ITR near the promoter region) was modified to eliminate the terminal resolution site and AAV D sequence. The resultant plasmid was named as scAAV-ARL3-EGFP. Triple-plasmid transfection into HEK293 cells was used to produce the AAV vector (58). The self-complementary ARL3-EGFP construct was packaged into AAV2/8 capsid. The vector was purified by polyethylene glycol precipitation followed by cesium chloride density gradient fractionation (58). The purified vector was maintained in solution containing 10 mM Tris-HCl, 180 mM NaCl, pH 7.4. The virus was titered by real time PCR using the following primers and fluorescent labeled probes: forward primer 5′-GCACCTTCTTGCCACTCCTA-3′ and reverse primer 5′-GACACAGCACCAGGCTAAATCC-3′; probe 5′-6-carboxyfluorescein-CGTCCTCCGTGACCCCGGC-tetramethylrhodamine-3′. Linearized plasmid DNA was used as standard to quantify the virus. In P15 WT and mutant mice, 0.5 μl of $3.9{\cdot}10^{12}$ ml^{-1} scAAV-ARL3-EGFP was injected subretinally, and the eyes were harvested at 2 months of age.

Statistics—SigmaPlot12 was used for statistical analysis using Student's *t* test, and the level of statistical significance was set to $p = 0.05$.

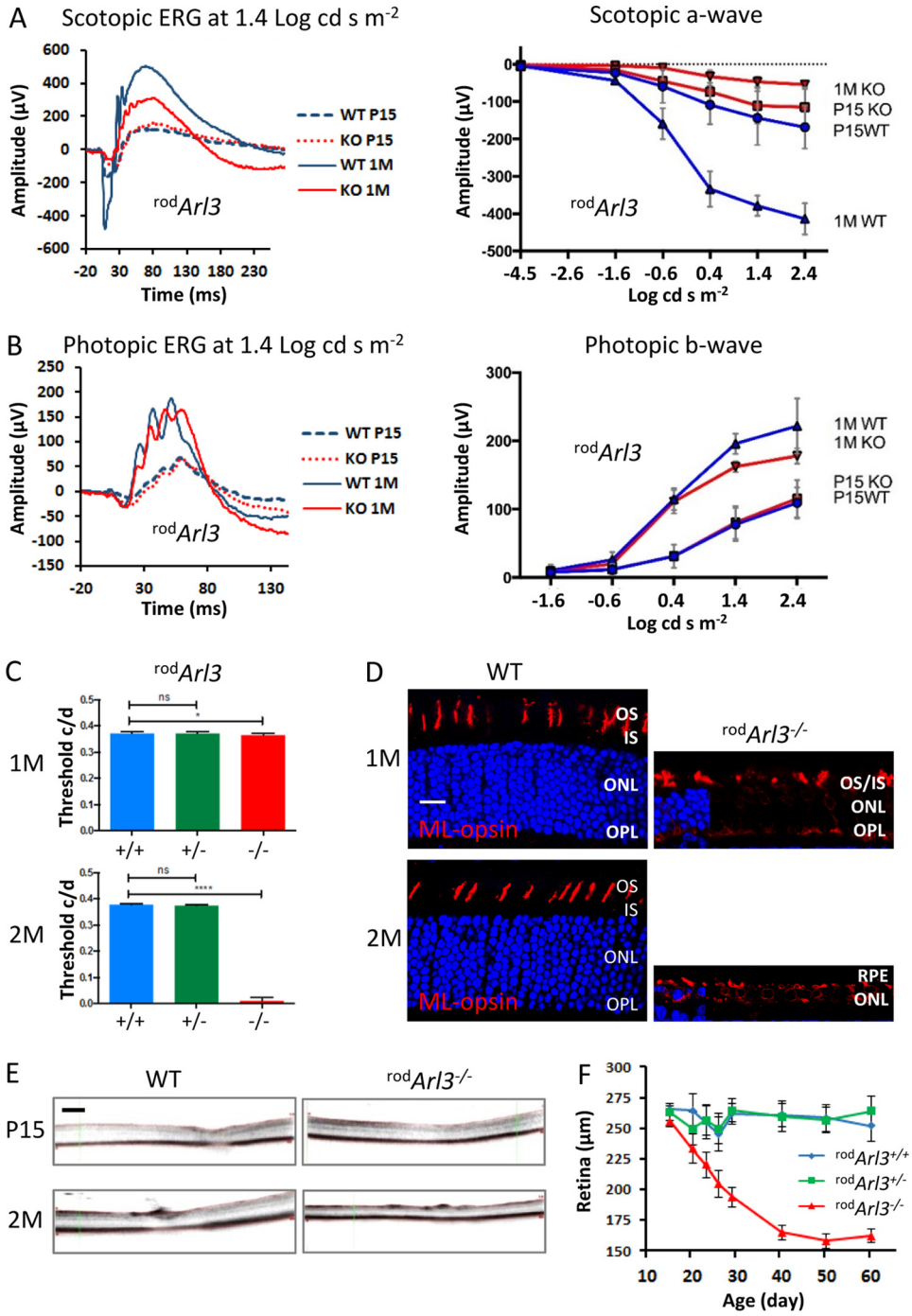

FIGURE 2. **Rod-specific *Arl3* knock-out.** *A,* scotopic ERG traces ($n = 7$) of P15 and 1-month (*M*)-old WT and $^{rod}Arl3^{-/-}$ mice at 1.4 log cds m^{-2}. Changes in a-wave amplitudes as a function of flash intensity are shown (*right panel*). *B,* photopic ERG traces ($n = 7$) of P15 and 1-month-old WT and $^{rod}Arl3^{-/-}$ mice at 1.4 log cds m^{-2}. Changes in b-wave amplitudes as a function of flash intensity are shown (*right panel*). *C,* OptoMotry ($n = 7$) of rod-specific knock-outs at 1 month (*top panel*) and 2 months (*bottom panel*) of age. Mutant OKT responses are plotted relative to heterozygous and WT controls. OKTs were comparable with controls in 1-month-old $^{rod}Arl3^{-/-}$ mice but were extinguished at 2 months of age with statistical significance ($p < 0.0001$). *D,* remnant $^{rod}Arl3^{-/-}$ cone outer segments, probed with anti-ML-opsin antibody (*red*), are present at 1 month (*top panel*) but not at 2 months (*bottom panel*), relative to WT littermates. *Scale bar,* 10 μm. *E,* WT and $^{rod}Arl3^{-/-}$ retina thickness measured by OCT at P15 (*top panel*) and 2 months (*bottom panel*). *Scale bar,* 200 μm. *F,* WT, $^{rod}Arl3^{+/-}$ and $^{rod}Arl3^{-/-}$ retina thickness as a function of age ($n = 3$), from P15 to P60. Retina degeneration starts at ~P15 in $^{rod}Arl3^{-/-}$ mice.

Results

Generation of Conditional Arl3 Knock-out Mice—Embryonic stem cells containing a β-GEO gene trap (52) in intron 1 of the mouse *Arl3* gene were used to generate chimeric mice (Fig. 1*A*). Before injection into blastocysts, position of the gene trap in intron 1 and presence of inverse FRT and loxP sites flanking the trap were confirmed by PCR and sequencing (Fig. 1*B*). The gene trap contains a splice-acceptor sequence upstream of the promoterless β-Geo reporter gene that essentially converts the gene trap into an exon. The trap is predicted to truncate ARL3 after exon 1, which ends after the start codon ATG, thereby preventing expression of ARL3. $Arl3^{GT/+}$ parents with verified

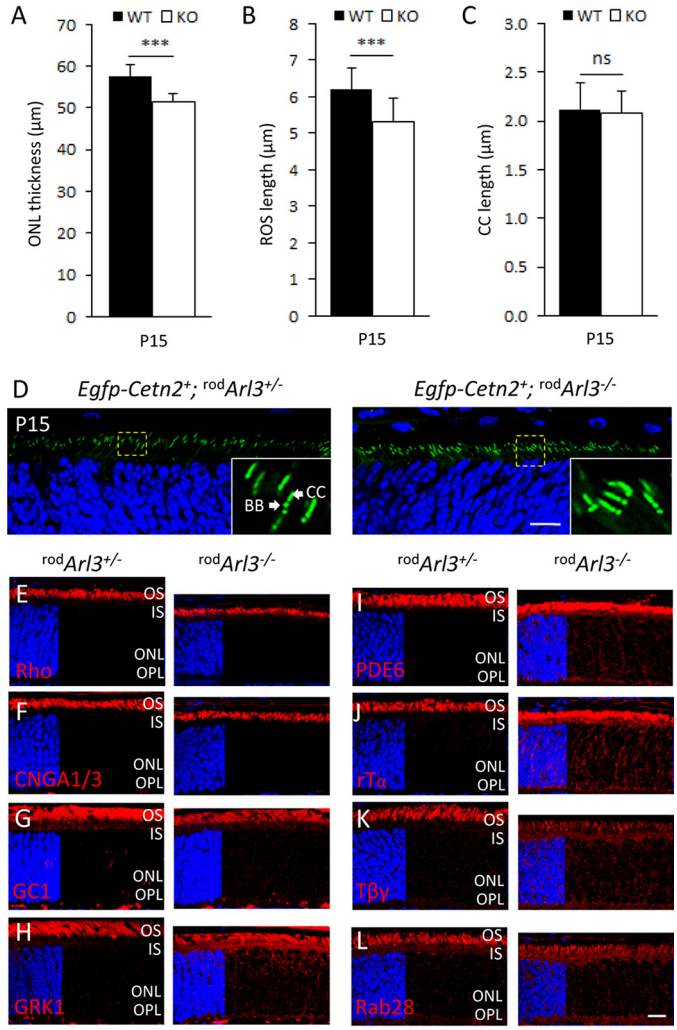

FIGURE 3. **Trafficking of transmembrane *versus* lipidated peripheral membrane proteins in rod-specific *Arl3* knock-out.** *A–C,* ONL thickness ($p < 0.001$) (*A*), ROS length ($p < 0.001$) (*B*), and intact connecting cilia (*C*). $^{rod}Arl3^{-/-}$ photoreceptors (*white bars*) are pre-degenerate at P15 ($n = 3$). *D,* centrioles and CC are identified by transgenic EGFP-CETN2. Mother (BB) and daughter centrioles form two adjacent *dots*, and the CC emerges as a tail from the BB. Note that the centriole/CC configuration is identical in $^{rod}Arl3^{+/-}$ and $^{rod}Arl3^{-/-}$. *E–L,* $^{rod}Arl3^{+/-}$ (*left panels*) and $^{rod}Arl3^{-/-}$ (*right panels*) mouse retina cryosections labeled with antibodies (*red*) directed against VPP-rhodopsin (*E*), CNGA1/3 (*F*), guanylate cyclase 1 (*GC1*) (*G*), GRK1 (*H*), PDE6 (*I*), rod Tα (*J*), rod Tβγ (*K*), and Rab28 (*L*). *D–L* were contrasted with DAPI (*blue*) to reveal the ONL. Trafficking of transmembrane proteins proceeds normally, whereas trafficking of PM proteins is severely impaired. *ns*, not significant. *Scale bar,* 10 μm.

germline transmission did not produce live $Arl3^{GT/GT}$ mice confirming embryonic or early postnatal embryonic lethality of $Arl3^{-/-}$ mice (46). In several $Arl3^{GT/+}$ matings, only 2 $Arl3^{GT/GT}$ mice (of 150) were born but did not survive (results not shown).

$Arl3^{GT/+}$ mice were mated with transgenic mice expressing flippase recombinase (*flp*), causing inversion of the gene trap (Fig. 1*C*). Inversion of the trap renders the gene trap inactive (no effect on ARL3 expression). Cre-loxP recombination was initiated with two transgenic lines, iCre75 mice expressing Cre recombinase (Cre) in rods (49, 56) or Six3-Cre mice expressing Cre in retinal progenitors (47). Cre-loxP recombination with iCre75 at postnatal day 7 (P7) and later inverted the trap only in rods to generate conditional rod knock-outs termed $^{rod}Arl3^{+/-}$, whereas Cre-loxP recombination with Six3-Cre inverted the trap in all retinal progenitors generating conditional retina knock-outs termed $^{ret}Arl3^{+/-}$ (Fig. 1*D*). Genotyping of offspring (Fig. 1*E*) and Western blot results (Fig. 1*F*) confirmed the generation of each conditional knock-out line. The *rd8* mutation of the *Crb1* gene (54) was detected in the F1 mutant mouse line but was subsequently eliminated by successive matings with *rd8*-free C57BL6/J mice.

Immunohistochemistry with available ARL3 antibodies was unsuccessful. To show the distribution of ARL3 unambiguously, we generated a self-complementary adeno-associated virus (scAAV2/8) expressing the fusion protein, ARL3-EGFP. Subretinal injection of scAAV-ARL3-EGFP revealed localization of ARL3, presumably in the GDP-bound form, throughout the outer nuclear layer (ONL), inner segment (IS), and connecting cilium (CC) but not the outer segment (Fig. 1*G*). ARL3 is likely in the GDP (inactive) form in the inner segments because its activating protein (GAP), RP2, is present in the inner segment cell membrane (41) and its GEF (which activates GDP/GTP exchange) is located at the connecting cilium and outer segment. ARL3-GTP is needed only at the ciliary ridge to unload cargo (see below). Enlargement of the IS/OS junction (Fig. 1*G*, *right panel*) reveals that ARL3 is enriched in the CC/BB area.

$^{rod}Arl3^{-/-}$ Photoreceptors Degenerate with RP-like Phenotype—During retina development, the mother centriole docks to the cortex of the rod IS around P5–6 to engage in ciliogenesis and axoneme formation (59). We initiated rod deletion of ARL3 by crossing $Arl3^{flox/flox}$ mice with iCre75 transgenic mice expressing Cre at P7 and later (49). Scotopic ERG recordings of P15 $^{rod}Arl3^{-/-}$ mice at various intensities (Fig. 2*A*) revealed nearly normal responses at P15 but reduced rod a- and b-wave amplitudes at 1 month of age. The presence of rod responses demonstrates that postnatal development, including ciliogenesis, occurred normally. The $^{rod}Arl3^{-/-}$ photopic responses (Fig. 2*B*) were robust and comparable with WT at P15 but started to decline (15–20%) at 1 month of age, a phenotype resembling RP. Visual function was further tested by Opto-Motry, a technique that enables the rapid screening of functional vision using the OKT response. At 1 month of age, $^{rod}Arl3^{-/-}$ OKT was normal but extinct at 2 months (Fig. 2*C*). The normal response at 1 month is most likely due to survival of cones (Fig. 2*D*, *right panel*). At 2 months of age, rods and cones were degenerated (Fig. 2, *D* and *F*), and the OKT response was extinguished. By optical coherence tomography (OCT), $^{rod}Arl3^{-/-}$ retina thickness declined at P15 (Fig. 2, *E* and *F*) and approached 160 μm at P50 (Fig. 2*F*). Heterozygous $^{rod}Arl3^{-/-}$ retina thickness (~260 μm) was identical to WT suggesting haplosufficiency (Fig. 2*F*). In mice expressing iCre75 on the WT background, retina thickness was unaffected over the first 60 postnatal days (56).

ARL3 Regulates Trafficking of Lipidated Peripheral Proteins—Based on ERG (Fig. 2, *A* and *B*), OKT (Fig. 2*C*), and retinal thickness (Fig. 2, *E* and *F*), $^{rod}Arl3^{-/-}$ retina presents a very early stage of degeneration at P15. ONL thickness (Fig. 3*A*) and rod outer segment length (Fig. 3*B*) are only slightly reduced, and connecting cilium length was normal (Fig. 3, *C* and *D*).

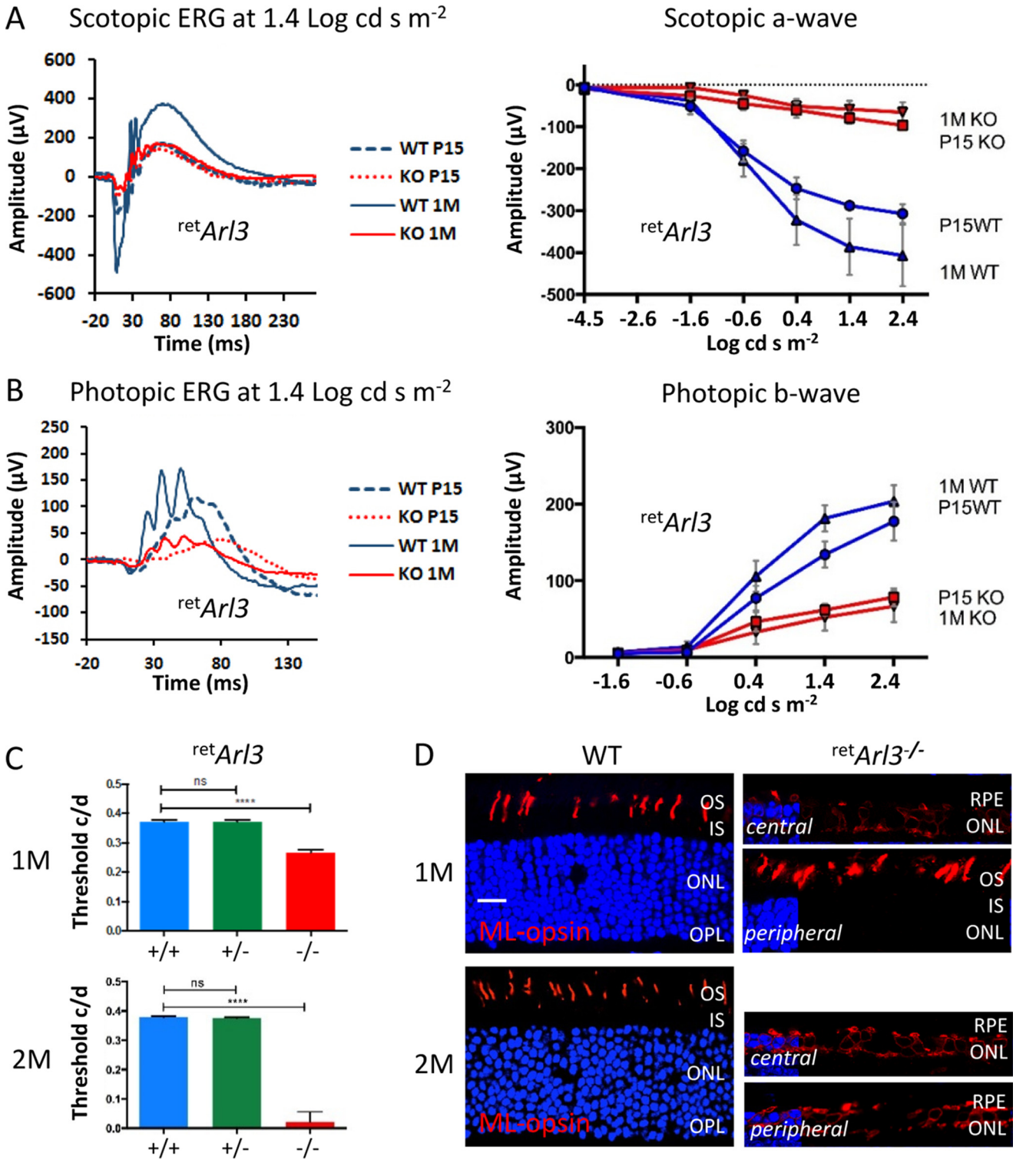

FIGURE 4. **Retina-specific *Arl3* deletion examined at time points P15 and 1 and 2 months.** *A,* scotopic $^{ret}Arl3^{-/-}$ ERG traces at 1.4 log cds m^{-2} ($n = 7$). Changes in a-wave amplitudes as a function of flash intensity are shown (*right panel*). *B,* photopic $^{ret}Arl3^{-/-}$ ERG traces at 1.4 log cds m^{-2} ($n = 7$). Changes in b-wave amplitudes as a function of flash intensity are shown (*right panel*). *C,* OptoMotry of retina-specific heterozygous and homozygous knock-outs ($n = 7$) at 1 month (*M*) (*top panel*) and 2 months of age (*bottom panel*). Optokinetic tracking responses were reduced in 1-month-old $^{ret}Arl3^{-/-}$ mice and nearly extinguished at 2 months of age, relative to heterozygous and WT controls ($p < 0.0001$). *D,* immunocytochemistry of 1-month-old (*top panel*) and 2-month-old (*bottom panel*) retina sections with anti-ML-opsin antibody (*red*) and DAPI (*blue*). Note that cone OS are present in the 1-month-old $^{ret}Arl3^{-/-}$ peripheral retina. *Scale bar,* 10 μm.

Connecting cilium, mother centriole (basal body), and daughter centriole were identified by expression of transgenic EGFP-CETN2 (Fig. 3*D*), a well characterized centriole (50) and connecting cilium marker (60). Transmembrane proteins, *e.g.* rhodopsin (Fig. 3*E*), rod/cone cGMP-gated channel α-subunits (CNGA1/3) (Fig. 3*F*), guanylate cyclase 1 (Fig. 3*G*), and cone

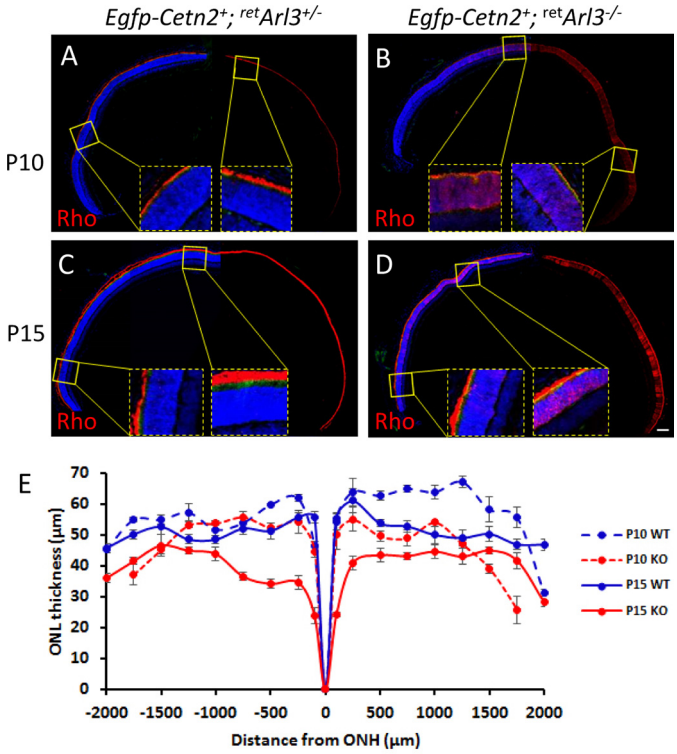

FIGURE 5. **Fluorescent immunohistochemistry of whole retina sections of WT and retina-specific *Arl3* knock-out retinas.** *A–D,* sections were labeled with anti-rhodopsin (*red*) and contrasted with DAPI (*blue*) to reveal nuclei, with enlargements of the central and peripheral retina. *Scale bar,* 100 μm. *E,* ONL thickness ($n = 3$) as the function of the distance from the optic nerve head (*ONH*).

pigments (M/L- and S-opsin, results not shown), trafficked normally and were unaffected by absence of ARL3. Farnesylated rhodopsin kinase (GRK1) (Fig. 3*H*), prenylated rod PDE6 (Fig. 3*I*), acylated rod Tα (Fig. 3*J*), farnesylated T$\beta\gamma$ (Fig. 3*K*), and Rab28 (Fig. 3*L*) mistrafficked to the inner segments, the ONL, and synaptic terminals. As a consequence, lipidated proteins accumulated in the ONL and inner segments of $^{rod}Arl3^{-/-}$ photoreceptors as inactivation of the *Arl3* gene by Cre-mediated recombination increased.

Retina-specific Deletion of ARL3—Six3-Cre-mediated recombination is expected to disable ARL3 expression as early as embryonic day 10 (47), before photoreceptor differentiation and ciliogenesis. Unexpectedly, $^{ret}Arl3^{-/-}$ scotopic and photopic ERG traces were recordable at P15 and 1 month (Fig. 4, *A* and *B*). The scotopic a-waves were suppressed at P15 and highly reduced at 1 month using flash intensities of -1.63 log cds m^{-2} and higher (Fig. 4*A, right panel*). Photopic b-waves were significantly reduced in P15 and 1-month-old animals to about 35% of normal ERG traces (Fig. 4*B, right panel*). The $^{ret}Arl3^{-/-}$ OKT response was 25% reduced at 1 month and nearly extinguished at 2 months (Fig. 4*C*). Significant visual activity in $^{ret}Arl3^{-/-}$ animals at 1 month may be due to survival mutant cones in the peripheral retina (Fig. 4*D, right panel*). ML-opsin-labeled cone outer segments were clearly present in the $^{ret}Arl3^{-/-}$ retina periphery, whereas OS were absent in the central $^{ret}Arl3^{-/-}$ retina. At 2 months, the $^{ret}Arl3^{-/-}$ retina was degenerated and unable to respond to light (Fig. 4*D*), a phenotype resembling Leber congenital amaurosis (61).

Six3-Cre-mediated recombination is known to be delayed in the retina periphery (60, 62). We therefore tested CC/OS formation by rhodopsin immunohistochemistry in the presence of EGFP-CETN2 at P10 and P15, the times when ERG and OKT showed significant visual responses. The results show normal OS in the peripheral $^{ret}Arl3^{-/-}$ retina, comparable with heterozygous controls, although degeneration in the central retina was far advanced (Fig. 5).

$^{ret}Arl3^{-/-}$ Rod and Cone Photoreceptors Do Not Form Outer Segments—OCT of $^{ret}Arl3^{-/-}$ animals showed a decrease in retina thickness to 200 μm as early as P15, further decreasing to ~160 μm at P30 (Fig. 6, *A* and *B*). ONL thickness is slightly reduced at P10, and active degeneration ensues at P15 (Fig. 6*C*). In control P10 and P15 $^{ret}Arl3^{+/-}$ retinas, connecting cilia formed as documented with the centriole/CC marker EGFP-CETN2 (Fig. 6, *D* and *E, left panels*). By contrast, in the P10 and P15 $^{ret}Arl3^{-/-}$ retinas, only mother and daughter centrioles were present, and functional basal bodies, connecting cilia and axonemes, were not formed (Fig. 6, *D* and *E, right panels*). Rhodopsin mislocalized throughout the ONL and IS (Fig. 6, *F* and *G*) similarly as observed in P10 $^{ret}Kif3a^{-/-}$ retina lacking connecting cilia and outer segments (60). Trafficking of lipidated proteins (PDE6) (Fig. 6, *H* and *I*), rod Tα (Fig. 6, *J* and *K*), and GRK1 (data not shown) was also impaired as outer segment disks are absent. Pigments M/L- and S-opsin distributed throughout the $^{ret}Arl3^{-/-}$ cones (Fig. 6, *L–O*). At P15, rod and cone photoreceptors degenerate massively (Fig. 6, *G, I, K, M,* and *O, right panels*). In contrast to phototransduction proteins, the ARL3 GEF ARL13b, which has an N-terminal palmitoylation motif and in *C. elegans* is palmitoylated (63), did not mislocalize in the $^{ret}Arl3^{-/-}$ ONL (Fig. 6, *P* and *Q*). ARL13b localization in the mutant retina is restricted to the apical IS and is presumably membrane-associated. The absence of outer segments as early as P10 in central $^{ret}Arl3^{-/-}$ photoreceptors suggests that ARL3, a known microtubule-interacting protein, may regulate a late stage of ciliogenesis or intraflagellar transport.

$^{ret}Arl3^{-/-}$ Versus $^{rod}Arl3^{-/-}$ Photoreceptor Degeneration—At P15, photoreceptor degeneration in $^{ret}Arl3^{-/-}$ mice proceeds faster than in $^{rod}Arl3^{-/-}$ mutants due to embryonic expression of Cre and lack of outer segments in the central retina (compare Figs. 3, *I–L,* and 6, *E–Q*). At 1 month, $^{ret}Arl3^{-/-}$ and $^{rod}Arl3^{-/-}$ photoreceptors degenerate rapidly with profound accumulation of PDE6, GRK1, and rod Tα in the remaining inner segments and ONL (Fig. 7, *A–C*). One-month-old $^{ret}Arl3^{-/-}$ and $^{rod}Arl3^{-/-}$ retinas reveal only 3–4 or 5–6 rows of ONL nuclei (Fig. 7, *A–C,* and *E*), respectively, and at 2 months the mutant retinas are both nearly completely degenerated (Fig. 7*F*).

Rescue of Ciliogenesis and Protein Trafficking in $^{ret}Arl3^{-/-}$ Photoreceptors—AAV particles expressing ARL3-EGFP were injected into the subretinal space of P15 WT and $^{ret}Arl3^{-/-}$ mice. Retinas harvested at 2 months post-injection (Fig. 8, *A–D*) show significant rescue of the ONL layer (4–5 rows of nuclei in treated *versus* 1 row in untreated retinas) (Fig. 8, *A–D, middle* and *right panels, E*). Moreover, treated central $^{ret}Arl3^{-/-}$ photoreceptors developed inner and outer segments, demonstrating rescue of ciliogenesis. Although outer

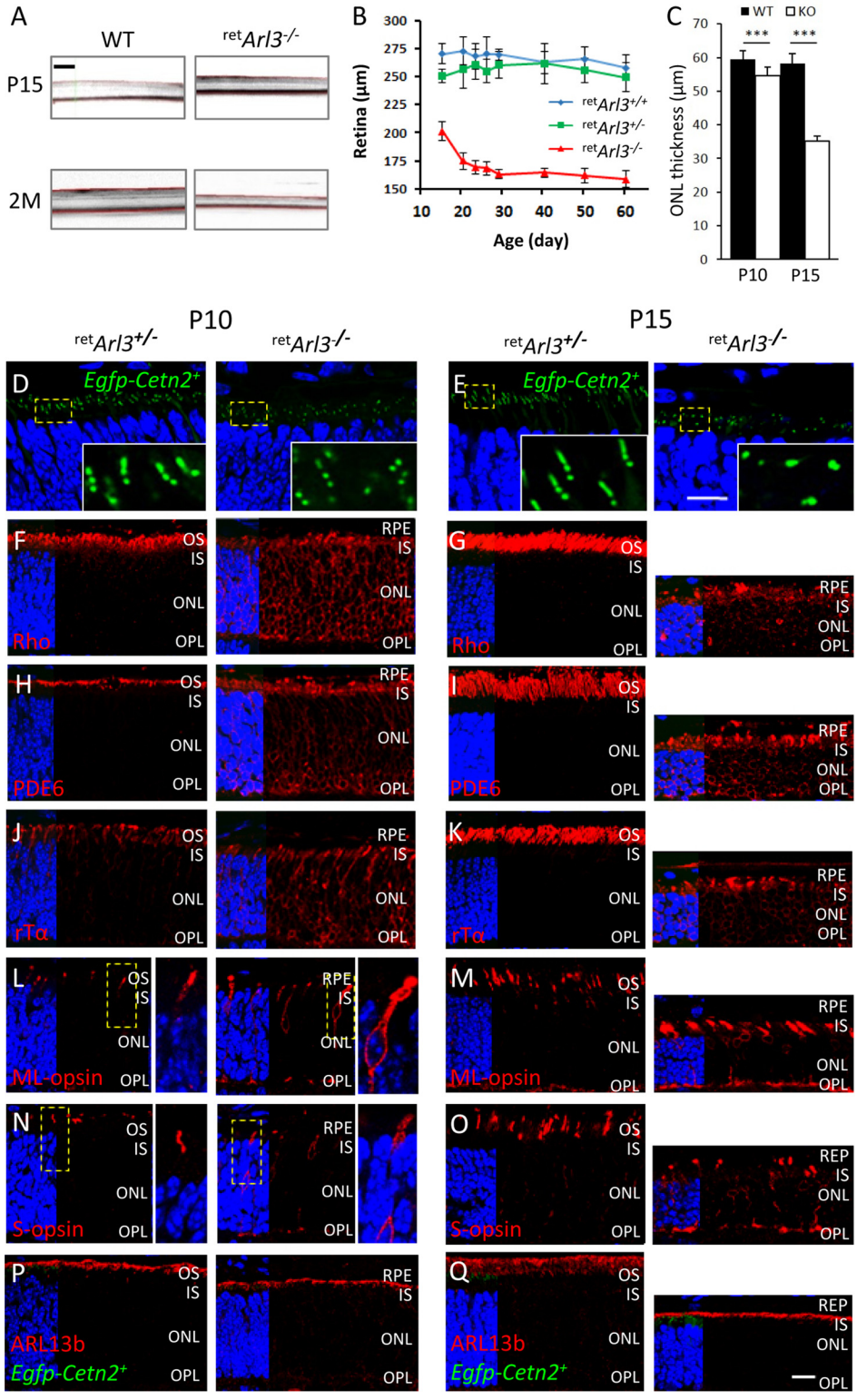

FIGURE 6. **Mistrafficking and degeneration in $^{ret}Arl3^{-/-}$ central photoreceptors.** *A,* OCT of WT (*left panel*) and $^{ret}Arl3^{-/-}$ (*right panel*) retinas at P15 (*top panel*) and 2 months (*bottom panel*). *B,* retina thickness measured by OCT as a function of age ($n = 3$). *C,* ONL thickness of WT (*black bars*) and mutant (*white bars*) mice at P10 and P15 ($p < 0.001$; $n = 3$). ***, $p < 0.001$. *D–Q,* retina immunohistochemistry at P10 (*left panel*) and P15 (*right panel*). Within each time point, heterozygote controls (*left panel*) are compared with knock-outs (*right panel*). *Panels* show EGFP-CETN2 fluorescence (*D* and *E*) or labeling with antibodies (*red*) directed against rhodopsin (*F* and *G*), PDE6 (*H* and *I*), rod Tα (*J* and *K*), ML-opsin (*L* and *M*), S-opsin (*N* and *O*), and ARL13b (*P* and *Q*). *Left quarter* of each panel show DAPI (*blue*) to identify extent of nuclear layer. *Scale bar,* 10 μm.

segments were shorter in treated retinas, outer segment proteins trafficked normally and did not mislocalize (Fig. 8, *A–D, middle panels*).

Trafficking of INPP5E to the Golgi—INPP5E is present in the cilia of hTert-RPE cells, cilia of mouse kidneys and cerebellum (64), and axonemes of mouse embryonic fibroblasts (26).

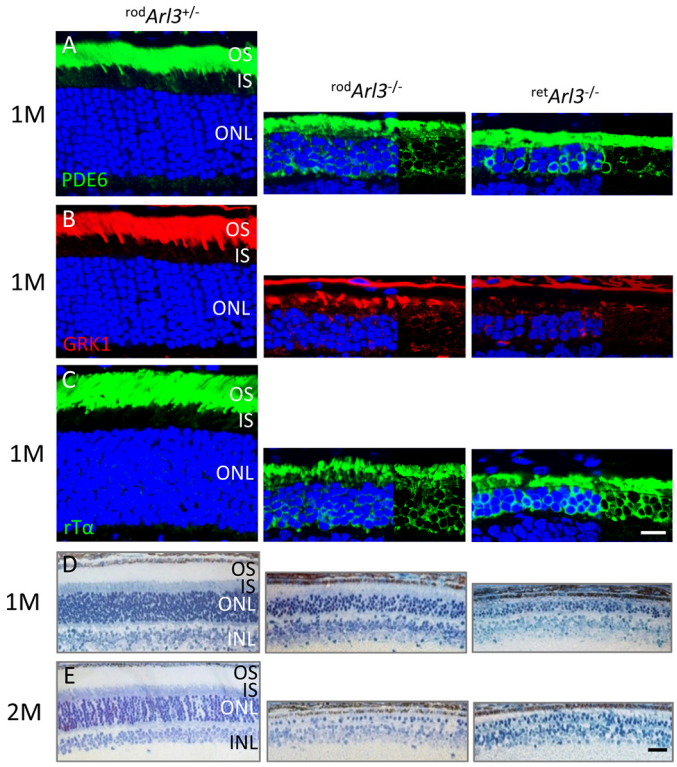

FIGURE 7. **Rapid degeneration of $^{rod}Arl3^{-/-}$ and $^{ret}Arl3^{-/-}$ rod photoreceptors at 1 and 2 months (*M*) of age.** *A–C*, sections of $^{rod}Arl3^{+/-}$, $^{rod}Arl3^{-/-}$, and $^{ret}Arl3^{-/-}$ retina were probed with anti-PDE6 (MOE) (*A*), anti-GRK1 (G8) (*B*), and anti-GNAT1 (rod Tα) antibodies (*C*). Rod outer segments in $Arl3^{-/-}$ sections are absent, and the ONL is reduced to ~5–6 rows in $^{rod}Arl3^{-/-}$ and 2–4 rows of nuclei in $^{ret}Arl3^{-/-}$. *Scale bar,* 10 μm. *D* and *E*, morphology of rod and retina knock-out animals at different ages. Plastic sections of 1 month (*D*) and 2 months (*E*) old heterozygous and homozygous knock-outs. *Arl3* mutant photoreceptors show rapid loss of outer segment and reduction of outer nuclear layers. At 2 months, each knock-out retina has only one nuclear row remaining in the ONL. *Scale bar,* 20 μm.

INPP5E is farnesylated and was suggested to travel to the OS in a PDEδ-dependent manner (25). In WT (data not shown) and $^{ret}Arl3^{+/-}$ mouse rods, however, INPP5E locates to the Golgi of inner segments and is absent in the outer segment (Fig. 9, *A* and *E*). At P10 when OS are forming, INPP5E is present in the inner segment proximal to centrioles, and rhodopsin localizes exclusively to the OS (Fig. 9, *A* and *B,* and *enlargements*). At P15 when OS are more developed, separation of rhodopsin and INPP5E fluorescence is most evident (Fig. 9, *E* and *F*). The enlargements reveal that centrioles and connecting cilia, identified by EGFP-CETN2, do not colocalize with INPP5E (Fig. 9*E*, *bottom panel*). In $^{ret}Arl3^{-/-}$ animals at P10 (Fig. 9, *C* and *D*) and P15 (Fig. 9, *G* and *H*), rhodopsin mislocalizes to the inner segments as outer segments are absent. INPP5E fluorescence of the $^{ret}Arl3^{-/-}$ IS appears significantly reduced (Fig. 9, *C* and *G*) compared with $^{ret}Arl3^{+/-}$ IS (Fig. 9, *A* and *E*), suggesting that INPP5E trafficking from ER-to-Golgi may in part be ARL3/PDEδ-dependent.

We generated an EGFP-INPP5E expression construct to avoid misinterpretation due to antibody artifacts. Neonatal electroporation of the construct and colabeling with a Golgi marker, anti-giantin, demonstrates that INPP5E distributes to the ER surrounding the nucleus and Golgi apparatus (Fig. 9, *I* and *J*), and it is excluded from WT and mutant outer segments (Fig. 9, *M* and *N*). In $^{ret}Arl3^{-/-}$ retina (Fig. 9, *K* and *L*), anti-giantin-labeled Golgi is retained in the degenerating ONL, and rhodopsin, unable to traffic, colocalizes with INPP5E (Fig. 9, *O* and *P*). The results show that farnesylated INPP5E traffics to the Golgi and not the outer segment of both WT and mutant photoreceptors.

Discussion

ARL3 is a small GTPase colocalizing with microtubules in HeLa cells and brain (40). The best-known function of ARL3, in the GTP-bound form, is that of a cargo displacement factor that evicts lipidated cargo from its lipid-binding protein (37, 38, 65). ARL3-dependent lipid-binding proteins are PDEδ and UNC119 featuring immunoglobulin-like β-sandwich structures that can accommodate lipid side chains with high affinity. However, germline $Arl3^{-/-}$ mice exhibited abnormal development of renal, hepatic, and pancreatic epithelial tubule structures, implicating ARL3 in ciliogenesis (46) and syndromic ciliopathy. To explore the role of ARL3 in photoreceptors, we generated rod- and retina-specific *Arl3* knock-outs. An advantage of the rod-specific knock-out is that Cre recombinase is expressed relatively late (>P7), after ciliogenesis has occurred, allowing $^{rod}Arl3^{-/-}$ rod outer segments to form normally. We observed significant mistrafficking of lipidated proteins as early as P15 (Fig. 3, *H–L, right panels*), signaling the onset of an RP-like photoreceptor degeneration. Rhodopsin and other transmembrane proteins are unaffected by loss of ARL3. In the WT scenario, lipidated cargo, docked to the ER membrane post-biosynthesis, is extracted by its lipid-binding protein (PDEδ or UNC119) and forms a soluble complex (Fig. 10*A*). The complex interacts with its CDF (ARL3-GTP), expelling cargo from its binding site and delivering it to the destination membrane. The phenotype of the rod-specific *Arl3* knock-out is consistent with loss of CDF function (Fig. 10*B*). In the absence of ARL3, lipidated cargo is retained and not delivered to the destination membrane, leading to accumulation of lipidated proteins in the IS and ONL (Figs. 3, *H–L,* and 10*B*). Non-delivery of PDE6 to the outer segment poses significant problems by upsetting the PDE6/guanylate cyclase cGMP regulatory system and shifting free cGMP to higher levels. As a result, rods degenerate with an RP-like phenotype that eventually affects cones as well (66).

Homozygous *RP2* null alleles in humans cause severe X-linked RP (XLGRP), whereas *Rp2* deletion in mice promotes a slowly progressing retinal degeneration (41, 67). We proposed that an abundance of dominantly active ARL3-GTP, stabilized by negligible intrinsic GTPase activity, attenuates the ability of PDEδ to interact with prenylated cargo (41). Interaction of ARL3-GTP with its PDEδ complex constricts the lipid-binding site and impairs the binding of cargo (alternatively, for UNC119, the binding pocket widens). Failure to extract cargo from the ER steadily lowers the concentration of lipidated proteins in the OS, initiating a slowly progressing photoreceptor degeneration. The $^{rod}Arl3^{-/-}$ trafficking defects are distinct from the $Rp2^{-/-}$ mouse defects where ARL3 is locked in the GTP-bound form thereby impeding extraction of PDE6 and GRK1 from the ER and leading to the degradation of the lipidated proteins (41). Over-

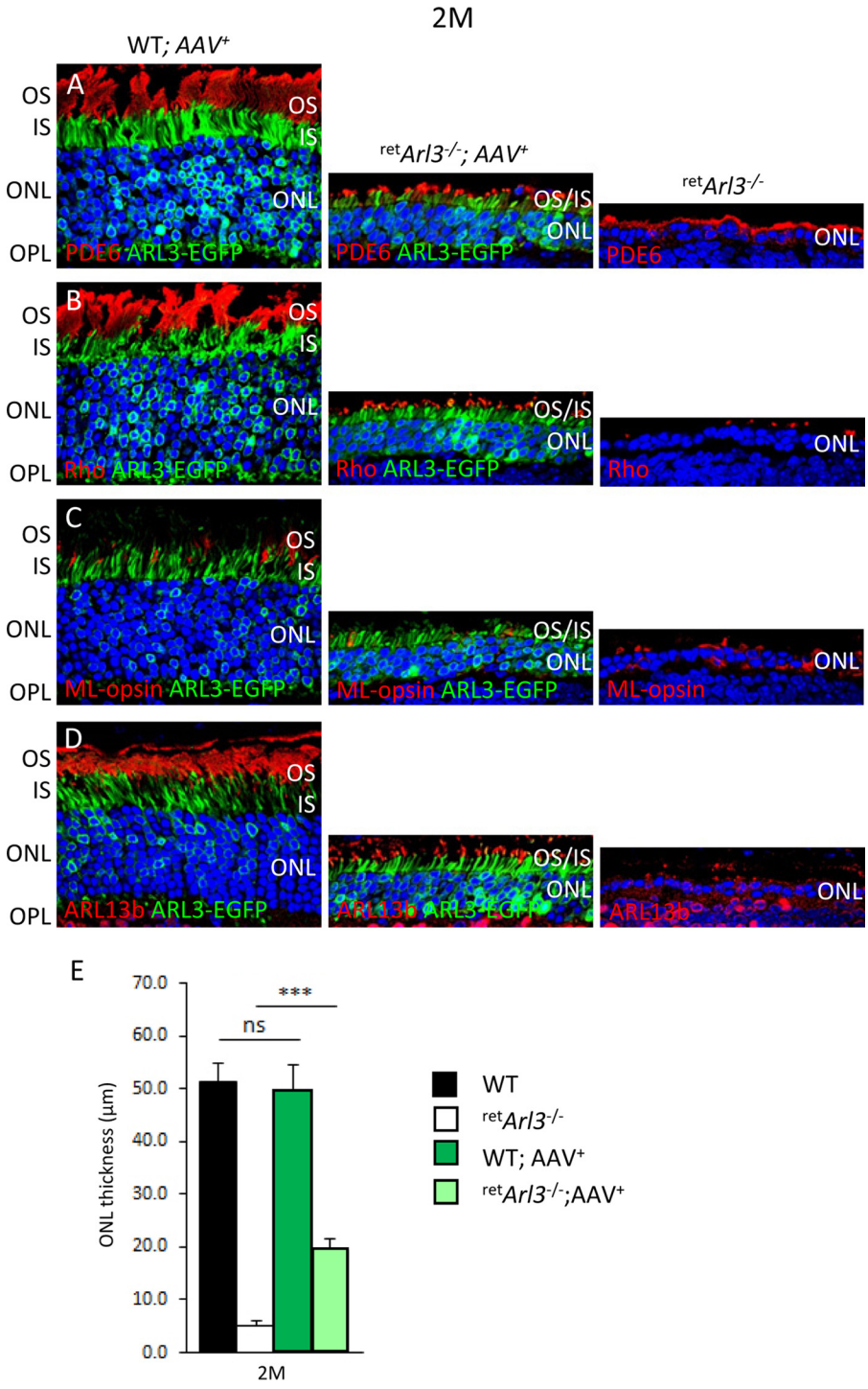

FIGURE 8. **Rescue of $^{ret}Arl3^{-/-}$ photoreceptor degeneration by scAAV-ARL3-EGFP.** *A–D,* frozen section of $^{ret}Arl3^{-/-}$ retina injected subretinally with scAAV-ARL3-EGFP at postnatal day P15 and harvested at 2 months post-injection. Photoreceptor outer segments were identified with anti-PDE6 (*A, red*), anti-rhodopsin (*B*), anti-ML-opsin (*C*), and anti-ARL13b (*D*) antibodies (*red*). Nuclei were counterstained with DAPI (*blue*). ARL3-EGFP localized to inner segments and perinuclearly to ER membranes, as shown in Fig. 1*G*. Note rescue of ciliogenesis, CC, IS, and OS formation in *A–D, middle panels*. *Scale bar,* 10 μm. *E,* evaluation of ONL thickness (μm) of indicated genotypes at 2 months post-injection ($n = 3$). ***, $p < 0.001$; *ns,* not significant.

expression of dominantly active ARL3 in *C. elegans* and *Leishmania* also causes ciliogenesis defects (30, 68), but mistrafficking of lipidated proteins has not been invoked as causal.

The severe ciliopathy phenotype of *Arl3* germline knockouts prompted us to investigate the consequence of ARL3 deletion during embryonic and early postnatal development, before the onset of ciliogenesis. Using transgenic EGFP-CETN2 as centriole and connecting cilium marker, we observed that connecting cilia (transition zones) and axonemes were undetectable in the central P10 $^{ret}Arl3^{-/-}$ retina, and the outer segments never form (Figs. 5 and 6, *D* and *E*). As an immediate consequence, transmembrane and peripheral membrane outer segment polypeptides accumulated in the inner segment (Fig. 6, *D–Q*). Although severe retinal degeneration was obvious at

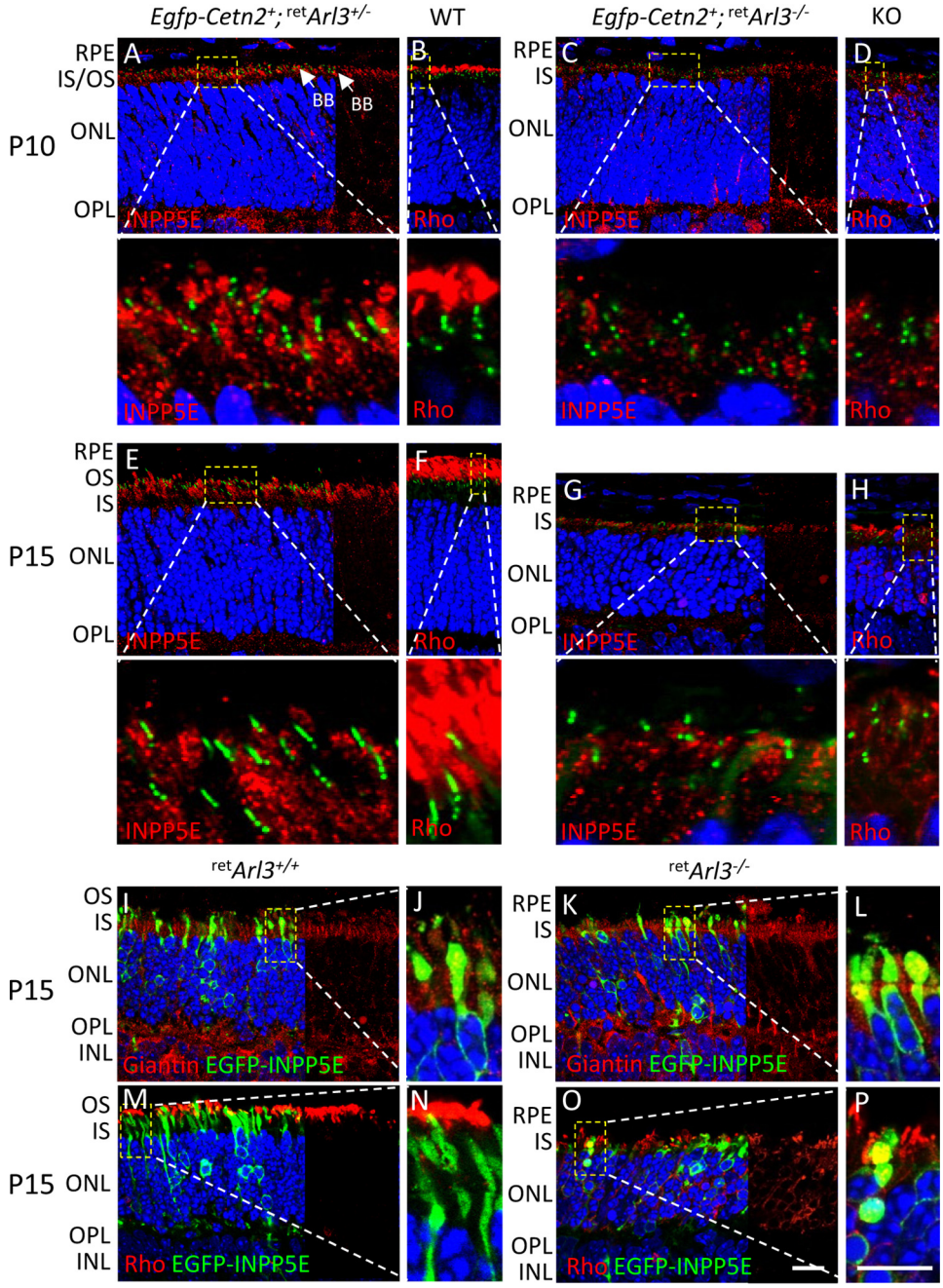

FIGURE 9. **INPP5E labels photoreceptor Golgi.** *A* and *B*, P10 *Egfp-Cetn2*$^{+}$;^{ret}*Arl3*$^{+/-}$ sections labeled with anti-INPP5E (*A*, *red*) or anti-rhodopsin (*B*, *red*). *Bottom panels*, enlargements as indicated. *C* and *D*, P10 *Egfp-Cetn2*$^{+}$;^{ret}*Arl3*$^{-/-}$ sections probed with anti-INPP5E (*C*) or anti-rhodopsin (*D*). IS/OS enlargements are shown *below each panel*. *E* and *F*, P15 *Egfp-Cetn2*$^{+}$;^{ret}*Arl3*$^{+/-}$ section labeled as shown in *A* and *B*. *Bottom panels*, enlargements as indicated. *G* and *H*, P15 *Egfp-Cetn2*$^{+}$;^{ret}*Arl3*$^{-/-}$ section probed as in *C* and *D*. *Bottom panels*, enlargements as indicated. *I–L*, P15 ^{ret}*Arl3*$^{+/+}$ (*I*) and ^{ret}*Arl3*$^{-/-}$ (*K*) sections labeled with anti-giantin (*red*) and EGFP-INPP5E (*green*), with enlargements (*right panels*). *Scale bar*, 10 μm. *J* and *L* are enlargements of *I* and *K*. *M–P*, P15 ^{ret}*Arl3*$^{+/+}$ (*M*) and ^{ret}*Arl3*$^{-/-}$ (*O*) sections labeled with anti-rhodopsin (*red*) and EGFP-INPP5E (*green*). *Scale bar*, 10 μm. *N* and *P* are enlargements of *M* and *O*, respectively.

P10, ciliogenesis in central ^{ret}*Arl3*$^{-/-}$ photoreceptors could be ameliorated by viral expression of ARL3 tagged with EGFP (Fig. 8). Although rescue of degeneration was only partial, inner segment and shortened outer segments were present in treated retinas demonstrating rescue of ciliogenesis and protein trafficking. Compartmentalization of ARL3 in the IS/basal body area and of its GEF, ARL13b, in the OS suggests that ARL3 must be switched into its GTP-bound active conformation to enable ciliogenesis. Accordingly, mutations in the human *ARL13b* gene disabling GEF activity on ARL3 and germline knock-out of the mouse *Arl13b* gene cause Joubert syndrome (44, 45).

The ^{ret}*Arl3*$^{-/-}$ phenotype is strikingly similar to a retina-specific knock-out of KIF3A (obligatory subunit of the heterotrimeric kinesin-2, KIF3) and IFT88 (particle of the IFT-B complex) (60). KIF3 and IFT88 are responsible for IFT of tubulin and axoneme building blocks. In ^{ret}*Kif3a*$^{-/-}$ rod and cone photoreceptors, ciliogenesis was disabled as early as P6 in the central retina, with a delay in the peripheral retina. A link between

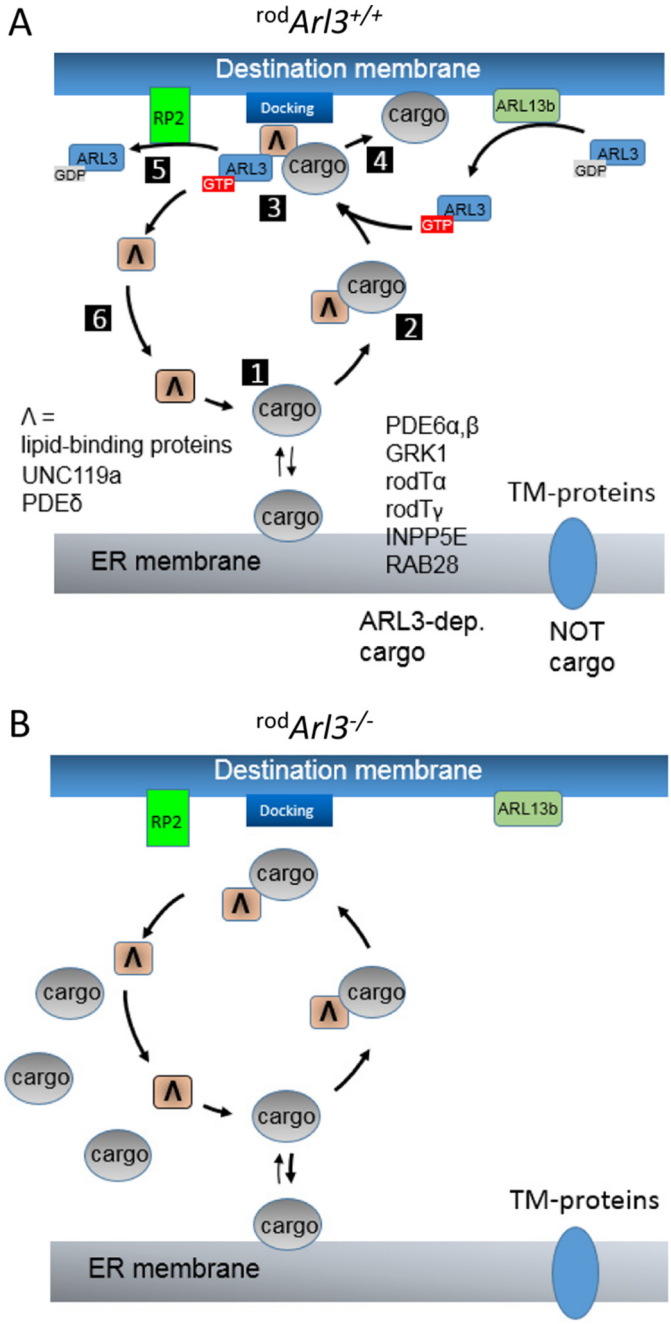

FIGURE 10. **Model of photoreceptor ARL3-dependent trafficking of lipidated cargo.** *A,* after biosynthesis, prenylated or acylated cargo docks to the ER membrane. Cargo dissociates (*1*) or is extracted by a lipid-binding protein (PDEδ or UNC119) and forms a diffusible complex (*2*). ARL3-GTP binds to the complex (*3*) and expels cargo from the lipid-binding protein for delivery to the destination membrane (*4*). The ternary complex falls apart; RP2 (GAP of ARL3) accelerates hydrolysis of GTP to GDP (*5*); and the lipid-binding protein is free to start another cycle (*6*). GDP/GTP exchange catalyzed by the membrane-bound GEF ARL13b regenerates ARL3-GTP. *B,* absence of ARL3 prevents delivery of cargo to the destination membrane, and cargo accumulates in the inner segments (Fig. 3).

ARL3 and intraflagellar transport was observed in *Leishmania* and *C. elegans*. In *Leishmania*, ARL3 is required for flagella formation (69), and in *C. elegans* ARL13b and ARL3 regulate IFT through a tubulin deacetylase (HDAC6) pathway (28, 68). In *Arl3* mutant worms, which have no GEF activity and presumably lack ARL3-GTP, IFTA, and IFTB, particles dissociate and disrupt IFT (28) suggesting that ARL3-GTP may be required for assembly of IFT complexes.

Finally, we investigated the trafficking of INPP5E in photoreceptors, dependence on ARL3/PDEδ, and function as a phosphatidylinositol-5′-phosphatase. Mutations in the human *INPP5E* gene are linked to Joubert and MORM syndromes (26, 64), and depletion of INPP5E in the adult mouse by tamoxifen induction causes rapid photoreceptor degeneration (26), suggesting a key role for phosphoinositide metabolism in ciliary maintenance. INPP5E, originally cloned from Golgi membranes, was shown to be predominantly located to the COS-7 Golgi (70). Among ciliated cells, INPP5E colocalized with acetylated α-tubulin in hTert-RPE cells, localized to cilia of P10 mouse kidneys and P5 cerebellum (64), and is concentrated in the axoneme of mouse embryonic fibroblasts (26). In IMCD3 cells, targeting to Golgi was proposed to be PDEδ/ARL3-dependent, whereas targeting to cilia was ARL13b-dependent (71). Absence of PDEδ prevented delivery of INPP5E to mouse embryonic fibroblast cilia, and a *PDE6D* null allele was linked to Joubert syndrome (25).

INPP5E was absent in mouse photoreceptor outer segments and apical inner segments and instead localized to the proximal inner segment and Golgi (Fig. 9, *A–H*). This is surprising, as INPP5E localizes along the axoneme of ciliated cells (26). Furthermore, PDEδ-mediated trafficking of INPP5E to the OS was suggested to be impaired in patients carrying a PDE6D null allele (25). Absence of INPP5E in the OS and its localization to the Golgi implies a critical role for INPP5E in the latter organelle. INPP5E levels in the $^{ret}Arl3^{-/-}$ inner segment/Golgi were reduced, suggesting that ER-to-Golgi trafficking of INPP5E may be ARL3/PDEδ-dependent. ARL13b, localizing exclusively to WT and $^{ret}Arl3^{-/-}$ OS (Fig. 6, *P* and *Q*), was suggested to target INPP5E to the OS (71). Distinct localizations of ARL13b in the OS and INPP5E in the Golgi discount this putative pathway.

The physiological role of INPP5E in the photoreceptor Golgi is intriguing as the Golgi is an organelle in which phosphatidylinositol 4-phosphate (PI4P) is enriched (72–74). PI4P could be generated by INPP5E-mediated hydrolysis of 5-phosphate bound to the inositol ring in phosphatidylinositol 4,5-bisphosphate or by 4′-phosphorylation of phosphatidylinositol by phosphatidylinositol 4-kinase. Interestingly, phosphatidylinositol 4-kinase knockdown abrogated Golgi to plasma membrane trafficking in mammalian cells (75) suggesting a key role for PI4P in vesicular trafficking. Reduction of INPP5E in the Golgi could deplete PI4P and impair Golgi-to-OS trafficking of membrane proteins, including rhodopsin, a protein that is essential for OS elaboration and vision.

Author Contributions—C. H. G., J. M. F., and H. Z. generated data; Z. W. generated the AAV virus expressing ARL3-EGFP; C. D. G. generated the polyclonal anti-ARL3 antibody; H. Z. and W. B. designed the knock-out strategy; C. H. G. and W. B. wrote the paper.

Acknowledgments—We thank Dr. Guoxin Ying (University of Utah) for expert help with neonatal electroporation and Dr. Judd Cahoon (University of Utah) for OCT expertise. We also thank Dr. Robert Seckler (University of Potsdam, Germany) for providing support to C. H. G. for off-site graduate project study.

References

1. Wright, A. F., Chakarova, C. F., Abd El-Aziz, M. M., and Bhattacharya, S. S. (2010) Photoreceptor degeneration: genetic and mechanistic dissection of a complex trait. *Nat. Rev. Genet.* **11,** 273–284
2. Lamb, T. D., and Pugh, E. N., Jr. (2006) Phototransduction, dark adaptation, and rhodopsin regeneration the proctor lecture. *Invest. Ophthalmol. Vis. Sci.* **47,** 5137–5152
3. Palczewski, K., and Benovic, J. L. (1991) G-protein-coupled receptor kinases. *Trends Biochem. Sci.* **16,** 387–391
4. Maeda, T., Imanishi, Y., and Palczewski, K. (2003) Rhodopsin phosphorylation: 30 years later. *Prog. Retin. Eye. Res* **22,** 417–434
5. Baehr, W., Morita, E. A., Swanson, R. J., and Applebury, M. L. (1982) Characterization of bovine rod outer segment G protein. *J. Biol. Chem.* **257,** 6452–6460
6. Fung, B. K. (1983) Characterization of transducin from bovine retinal rod outer segments. I. Separation and reconstitution of the subunits. *J. Biol. Chem.* **258,** 10495–10502
7. Lerea, C. L., Somers, D. E., Hobson, A., Raport, C. J., Bunt-Milam, A. H., and Hurley, J. B. (1987) Photoreceptor G-proteins. *Prog. Clin. Biol. Res.* **249,** 31–41
8. Arshavsky, V. Y., Lamb, T. D., and Pugh, E. N., Jr. (2002) G proteins and phototransduction. *Annu. Rev. Physiol.* **64,** 153–187
9. Baehr, W., Devlin, M. J., and Applebury, M. L. (1979) Isolation and characterization of cGMP phosphodiesterase from bovine rod outer segments. *J. Biol. Chem.* **254,** 11669–11677
10. Kameni Tcheudji, J. F., Lebeau, L., Virmaux, N., Maftei, C. G., Cote, R. H., Lugnier, C., and Schultz, P. (2001) Molecular organization of bovine rod cGMP-phosphodiesterase 6. *J. Mol. Biol.* **310,** 781–791
11. Anant, J. S., Ong, O. C., Xie, H. Y., Clarke, S., O'Brien, P. J., and Fung, B. K. (1992) *In vivo* differential prenylation of retinal cyclic GMP phosphodiesterase catalytic subunits. *J. Biol. Chem.* **267,** 687–690
12. Inglese, J., Glickman, J. F., Lorenz, W., Caron, M. G., and Lefkowitz, R. J. (1992) Isoprenylation of a protein kinase. Requirement of farnesylation/α-carboxyl methylation for full enzymatic activity of rhodopsin kinase. *J. Biol. Chem.* **267,** 1422–1425
13. Qin, N., Pittler, S. J., and Baehr, W. (1992) *In vitro* isoprenylation and membrane association of mouse rod photoreceptor cGMP phosphodiesterase α and β subunits expressed in bacteria. *J. Biol. Chem.* **267,** 8458–8463
14. Inglese, J., Koch, W. J., Caron, M. G., and Lefkowitz, R. J. (1992) Isoprenylation in regulation of signal transduction by G-protein-coupled receptor kinases. *Nature* **359,** 147–150
15. Lai, R. K., Perez-Sala, D., Cañada, F. J., and Rando, R. R. (1990) The γ subunit of transducin is farnesylated. *Proc. Natl. Acad. Sci. U.S.A.* **87,** 7673–7677
16. Yang, Z., and Wensel, T. G. (1992) *N*-Myristoylation of the rod outer segment G protein, transducin, in cultured retinas. *J. Biol. Chem.* **267,** 23197–23201
17. Liebman, P. A., and Entine, G. (1974) Lateral diffusion of visual pigment in photoreceptor disk membranes. *Science* **185,** 457–459
18. Calvert, P. D., Govardovskii, V. I., Krasnoperova, N., Anderson, R. E., Lem, J., and Makino, C. L. (2001) Membrane protein diffusion sets the speed of rod phototransduction. *Nature* **411,** 90–94
19. Young, R. W. (1976) Visual cells and the concept of renewal. *Invest. Ophthalmol. Vis. Sci.* **15,** 700–725
20. Anderson, D. H., Fisher, S. K., and Steinberg, R. H. (1978) Mammalian cones: disc shedding, phagocytosis, and renewal. *Invest. Ophthalmol. Vis. Sci.* **17,** 117–133
21. Marrari, Y., Crouthamel, M., Irannejad, R., and Wedegaertner, P. B. (2007) Assembly and trafficking of heterotrimeric G proteins. *Biochemistry* **46,** 7665–7677
22. Zhang, H., Li, S., Doan, T., Rieke, F., Detwiler, P. B., Frederick, J. M., and Baehr, W. (2007) Deletion of PrBP/δ impedes transport of GRK1 and PDE6 catalytic subunits to photoreceptor outer segments. *Proc. Natl. Acad. Sci. U.S.A.* **104,** 8857–8862
23. Baehr, W. (2014) Membrane protein transport in photoreceptors: the function of PDEdelta: the Proctor lecture. *Invest. Ophthalmol. Vis. Sci.* **55,** 8653–8666
24. Zhang, H., Constantine, R., Vorobiev, S., Chen, Y., Seetharaman, J., Huang, Y. J., Xiao, R., Montelione, G. T., Gerstner, C. D., Davis, M. W., Inana, G., Whitby, F. G., Jorgensen, E. M., Hill, C. P., Tong, L., and Baehr, W. (2011) UNC119 is required for G protein trafficking in sensory neurons. *Nat. Neurosci.* **14,** 874–880
25. Thomas, S., Wright, K. J., Le, C. S., Micalizzi, A., Romani, M., Abhyankar, A., Saada, J., Perrault, I., Amiel, J., Litzler, J., Filhol, E., Elkhartoufi, N., Kwong, M., Casanova, J. L., Boddaert, N., *et al.* (2014) A homozygous PDE6D mutation in Joubert syndrome impairs targeting of farnesylated INPP5E protein to the primary cilium. *Hum. Mutat.* **35,** 137–146
26. Jacoby, M., Cox, J. J., Gayral, S., Hampshire, D. J., Ayub, M., Blockmans, M., Pernot, E., Kisseleva, M. V., Compère, P., Schiffmann, S. N., Gergely, F., Riley, J. H., Pérez-Morga, D., Woods, C. G., and Schurmans, S. (2009) INPP5E mutations cause primary cilium signaling defects, ciliary instability and ciliopathies in human and mouse. *Nat. Genet.* **41,** 1027–1031
27. Kobayashi, A., Higashide, T., Hamasaki, D., Kubota, S., Sakuma, H., An, W., Fujimaki, T., McLaren, M. J., Weleber, R. G., and Inana, G. (2000) HRG4 (UNC119) mutation found in cone-rod dystrophy causes retinal degeneration in a transgenic model. *Invest. Ophthalmol. Vis. Sci.* **41,** 3268–3277
28. Zhang, Q., Hu, J., and Ling, K. (2013) Molecular views of Arf-like small GTPases in cilia and ciliopathies. *Exp. Cell Res.* **319,** 2316–2322
29. Cavenagh, M. M., Breiner, M., Schurmann, A., Rosenwald, A. G., Terui, T., Zhang, C., Randazzo, P. A., Adams, M., Joost, H. G., and Kahn, R. A. (1994) ADP-ribosylation factor (ARF)-like 3, a new member of the ARF family of GTP-binding proteins cloned from human and rat tissues. *J. Biol. Chem.* **269,** 18937–18942
30. Cuvillier, A., Redon, F., Antoine, J. C., Chardin, P., DeVos, T., and Merlin, G. (2000) LdARL-3A, a *Leishmania* promastigote-specific ADP-ribosylation factor-like protein, is essential for flagellum integrity. *J. Cell Sci.* **113,** 2065–2074
31. Wright, K. J., Baye, L. M., Olivier-Mason, A., Mukhopadhyay, S., Sang, L., Kwong, M., Wang, W., Pretorius, P. R., Sheffield, V. C., Sengupta, P., Slusarski, D. C., and Jackson, P. K. (2011) An ARL3-UNC119-RP2 GTPase cycle targets myristoylated NPHP3 to the primary cilium. *Genes Dev.* **25,** 2347–2360
32. Linari, M., Hanzal-Bayer, M., and Becker, J. (1999) The δ subunit of rod specific cyclic GMP phosphodiesterase, PDE delta, interacts with the Arf-like protein Arl3 in a GTP specific manner. *FEBS Lett.* **458,** 55–59
33. Kobayashi, A., Kubota, S., Mori, N., McLaren, M. J., and Inana, G. (2003) Photoreceptor synaptic protein HRG4 (UNC119) interacts with ARL2 via a putative conserved domain. *FEBS Lett.* **534,** 26–32
34. Hanzal-Bayer, M., Renault, L., Roversi, P., Wittinghofer, A., and Hillig, R. C. (2002) The complex of Arl2-GTP and PDEδ: from structure to function. *EMBO J.* **21,** 2095–2106
35. Renault, L., Hanzal-Bayer, M., and Hillig, R. C. (2001) Coexpression, copurification, crystallization and preliminary x-ray analysis of a complex of ARL2-GTP and PDE δ. *Acta Crystallogr. D Biol. Crystallogr.* **57,** 1167–1170
36. Veltel, S., Gasper, R., Eisenacher, E., and Wittinghofer, A. (2008) The retinitis pigmentosa 2 gene product is a GTPase-activating protein for Arf-like 3. *Nat. Struct. Mol. Biol.* **15,** 373–380
37. Ismail, S. A., Chen, Y. X., Miertzschke, M., Vetter, I. R., Koerner, C., and Wittinghofer, A. (2012) Structural basis for Arl3-specific release of myristoylated ciliary cargo from UNC119. *EMBO J.* **31,** 4085–4094
38. Ismail, S. A., Chen, Y. X., Rusinova, A., Chandra, A., Bierbaum, M., Gremer, L., Triola, G., Waldmann, H., Bastiaens, P. I., and Wittinghofer, A. (2011) Arl2-GTP and Arl3-GTP regulate a GDI-like transport system for farnesylated cargo. *Nat. Chem. Biol.* **7,** 942–949
39. Schwarz, N., Hardcastle, A. J., and Cheetham, M. E. (2012) Arl3 and RP2 mediated assembly and traffic of membrane associated cilia proteins. *Vis. Res.* **75,** 2–4
40. Grayson, C., Bartolini, F., Chapple, J. P., Willison, K. R., Bhamidipati, A., Lewis, S. A., Luthert, P. J., Hardcastle, A. J., Cowan, N. J., and Cheetham, M. E. (2002) Localization in the human retina of the X-linked retinitis pigmentosa protein RP2, its homologue cofactor C and the RP2 interacting protein Arl3. *Hum. Mol. Genet.* **11,** 3065–3074

41. Zhang, H., Hanke-Gogokhia, C., Jiang, L., Li, X., Wang, P., Gerstner, C. D., Frederick, J. M., Yang, Z., and Baehr, W. (2015) Mistrafficking of prenylated proteins causes retinitis pigmentosa 2. *FASEB J.* **29,** 932–942
42. Ishiba, Y., Higashide, T., Mori, N., Kobayashi, A., Kubota, S., McLaren, M. J., Satoh, H., Wong, F., and Inana, G. (2007) Targeted inactivation of synaptic HRG4 (UNC119) causes dysfunction in the distal photoreceptor and slow retinal degeneration, revealing a new function. *Exp. Eye Res.* **84,** 473–485
43. Gotthardt, K., Lokaj, M., Koerner, C., Falk, N., Giessl, A., and Wittinghofer, A. (2015) A G-protein activation cascade from Arl13b to Arl3 and implications for ciliary targeting of lipidated proteins. *eLife* **4,** e11859
44. Cantagrel, V., Silhavy, J. L., Bielas, S. L., Swistun, D., Marsh, S. E., Bertrand, J. Y., Audollent, S., Attié-Bitach, T., Holden, K. R., Dobyns, W. B., Traver, D., Al-Gazali, L., Ali, B. R., Lindner, T. H., Caspary, T., *et al.* (2008) Mutations in the cilia gene ARL13B lead to the classical form of Joubert syndrome. *Am. J. Hum. Genet.* **83,** 170–179
45. Su, C. Y., Bay, S. N., Mariani, L. E., Hillman, M. J., and Caspary, T. (2012) Temporal deletion of Arl13b reveals that a mispatterned neural tube corrects cell fate over time. *Development* **139,** 4062–4071
46. Schrick, J. J., Vogel, P., Abuin, A., Hampton, B., and Rice, D. S. (2006) ADP-ribosylation factor-like 3 is involved in kidney and photoreceptor development. *Am. J. Pathol.* **168,** 1288–1298
47. Furuta, Y., Lagutin, O., Hogan, B. L., and Oliver, G. C. (2000) Retina- and ventral forebrain-specific Cre recombinase activity in transgenic mice. *Genesis* **26,** 130–132
48. Hayashi, S., and McMahon, A. P. (2002) Efficient recombination in diverse tissues by a tamoxifen-inducible form of Cre: a tool for temporally regulated gene activation/inactivation in the mouse. *Dev. Biol.* **244,** 305–318
49. Li, S., Chen, D., Sauvé, Y., McCandles, J., Chen, Y. J., and Chen, C.-K. (2005) Rhodopsin-iCre transgenic mouse line for Cre-mediated rod-specific gene targeting. *Genesis* **41,** 73–80
50. Higginbotham, H., Bielas, S., Tanaka, T., and Gleeson, J. G. (2004) Transgenic mouse line with green-fluorescent protein-labeled Centrin 2 allows visualization of the centrosome in living cells. *Transgenic. Res.* **13,** 155–164
51. Friedel, R. H., Wurst, W., Wefers, B., and Kühn, R. (2011) Generating conditional knock-out mice. *Methods Mol. Biol.* **693,** 205–231
52. Friedel, R. H., Seisenberger, C., Kaloff, C., and Wurst, W. (2007) EUCOMM–the European conditional mouse mutagenesis program. *Brief. Funct. Genomic. Proteomic.* **6,** 180–185
53. Bouabe, H., and Okkenhaug, K. (2013) Gene targeting in mice: a review. *Methods Mol. Biol.* **1064,** 315–336
54. Mattapallil, M. J., Wawrousek, E. F., Chan, C. C., Zhao, H., Roychoudhury, J., Ferguson, T. A., and Caspi, R. R. (2012) The Rd8 mutation of the Crb1 gene is present in vendor lines of C57BL/6N mice and embryonic stem cells, and confounds ocular induced mutant phenotypes. *Invest. Ophthalmol. Vis. Sci.* **53,** 2921–2927
55. Zhang, H., Fan, J., Li, S., Karan, S., Rohrer, B., Palczewski, K., Frederick, J. M., Crouch, R. K., and Baehr, W. (2008) Trafficking of membrane-associated proteins to cone photoreceptor outer segments requires the chromophore 11-cis-retinal. *J. Neurosci.* **28,** 4008–4014
56. Avasthi, P., Watt, C. B., Williams, D. S., Le, Y. Z., Li, S., Chen, C. K., Marc, R. E., Frederick, J. M., and Baehr, W. (2009) Trafficking of membrane proteins to cone but not rod outer segments is dependent on heterotrimeric kinesin-II. *J. Neurosci.* **29,** 14287–14298
57. Barabas, P., Huang, W., Chen, H., Koehler, C. L., Howell, G., John, S. W., Tian, N., Rentería, R. C., and Krizaj, D. (2011) Missing optomotor head-turning reflex in the DBA/2J mouse. *Invest. Ophthalmol. Vis. Sci.* **52,** 6766–6773
58. Grimm, D., Zhou, S., Nakai, H., Thomas, C. E., Storm, T. A., Fuess, S., Matsushita, T., Allen, J., Surosky, R., Lochrie, M., Meuse, L., McClelland, A., Colosi, P., and Kay, M. A. (2003) Preclinical *in vivo* evaluation of pseudotyped adeno-associated virus vectors for liver gene therapy. *Blood* **102,** 2412–2419
59. Avasthi, P., and Marshall, W. F. (2012) Stages of ciliogenesis and regulation of ciliary length. *Differentiation* **83,** S30–S42
60. Jiang, L., Wei, Y., Ronquillo, C. C., Marc, R. E., Yoder, B. K., Frederick, J. M., and Baehr, W. (2015) Kinesin-2 (KIF3) mediates transition zone and axoneme formation of mouse photoreceptors. *J. Biol. Chem.* **290,** 12765–12778
61. den Hollander, A. I., Roepman, R., Koenekoop, R. K., and Cremers, F. P. (2008) Leber congenital amaurosis: genes, proteins and disease mechanisms. *Prog. Retin. Eye Res.* **27,** 391–419
62. Zhang, J., Fuhrmann, S., and Vetter, M. L. (2008) A nonautonomous role for retinal frizzled-5 in regulating hyaloid vitreous vasculature development. *Invest. Ophthalmol. Vis. Sci.* **49,** 5561–5567
63. Cevik, S., Hori, Y., Kaplan, O. I., Kida, K., Toivenon, T., Foley-Fisher, C., Cottell, D., Katada, T., Kontani, K., and Blacque, O. E. (2010) Joubert syndrome Arl13b functions at ciliary membranes and stabilizes protein transport in *Caenorhabditis elegans*. *J. Cell Biol.* **188,** 953–969
64. Bielas, S. L., Silhavy, J. L., Brancati, F., Kisseleva, M. V., Al-Gazali, L., Sztriha, L., Bayoumi, R. A., Zaki, M. S., Abdel-Aleem, A., Rosti, R. O., Kayserili, H., Swistun, D., Scott, L. C., Bertini, E., Boltshauser, E., *et al.* (2009) Mutations in INPP5E, encoding inositol polyphosphate-5-phosphatase E, link phosphatidyl inositol signaling to the ciliopathies. *Nat. Genet.* **41,** 1032–1036
65. Veltel, S., Kravchenko, A., Ismail, S., and Wittinghofer, A. (2008) Specificity of Arl2/Arl3 signaling is mediated by a ternary Arl3-effector-GAP complex. *FEBS Lett.* **582,** 2501–2507
66. Hartong, D. T., Berson, E. L., and Dryja, T. P. (2006) Retinitis pigmentosa. *Lancet* **368,** 1795–1809
67. Li, L., Khan, N., Hurd, T., Ghosh, A. K., Cheng, C., Molday, R., Heckenlively, J. R., Swaroop, A., and Khanna, H. (2013) Ablation of the X-linked retinitis pigmentosa 2 (Rp2) gene in mice results in opsin mislocalization and photoreceptor degeneration. *Invest. Ophthalmol. Vis. Sci.* **54,** 4503–4511
68. Li, Y., Wei, Q., Zhang, Y., Ling, K., and Hu, J. (2010) The small GTPases ARL-13 and ARL-3 coordinate intraflagellar transport and ciliogenesis. *J. Cell Biol.* **189,** 1039–1051
69. Efimenko, E., Bubb, K., Mak, H. Y., Holzman, T., Leroux, M. R., Ruvkun, G., Thomas, J. H., and Swoboda, P. (2005) Analysis of xbx genes in *C. elegans*. *Development* **132,** 1923–1934
70. Kong, A. M., Speed, C. J., O'Malley, C. J., Layton, M. J., Meehan, T., Loveland, K. L., Cheema, S., Ooms, L. M., and Mitchell, C. A. (2000) Cloning and characterization of a 72-kDa inositol-polyphosphate 5-phosphatase localized to the Golgi network. *J. Biol. Chem.* **275,** 24052–24064
71. Humbert, M. C., Weihbrecht, K., Searby, C. C., Li, Y., Pope, R. M., Sheffield, V. C., and Seo, S. (2012) ARL13B, PDE6D, and CEP164 form a functional network for INPP5E ciliary targeting. *Proc. Natl. Acad. Sci. U.S.A.* **109,** 19691–19696
72. Wang, Y. J., Wang, J., Sun, H. Q., Martinez, M., Sun, Y. X., Macia, E., Kirchhausen, T., Albanesi, J. P., Roth, M. G., and Yin, H. L. (2003) Phosphatidylinositol 4 phosphate regulates targeting of clathrin adaptor AP-1 complexes to the Golgi. *Cell* **114,** 299–310
73. Conduit, S. E., Dyson, J. M., and Mitchell, C. A. (2012) Inositol polyphosphate 5-phosphatases; new players in the regulation of cilia and ciliopathies. *FEBS Lett.* **586,** 2846–2857
74. Nakatsu, F. (2015) A phosphoinositide code for primary cilia. *Dev. Cell* **34,** 379–380
75. Wang, J., Sun, H. Q., Macia, E., Kirchhausen, T., Watson, H., Bonifacino, J. S., and Yin, H. L. (2007) PI4P promotes the recruitment of the GGA adaptor proteins to the trans-Golgi network and regulates their recognition of the ubiquitin sorting signal. *Mol. Biol. Cell* **18,** 2646–2655